Simulations of Skin Barrier Function: Free Energies of Hydrophobic and Hydrophilic Transmembrane Pores in Ceramide Bilayers

Rebecca Notman,* Jamshed Anwar,† W. J. Briels,‡ Massimo G. Noro,§ and Wouter K. den Otter‡

*Molecular Biophysics, Division of Pharmaceutical Science, King's College London, London, United Kingdom; †Computational Biophysics Laboratory, Institute of Pharmaceutical Innovation, University of Bradford, Bradford, United Kingdom; ‡Computational Biophysics, University of Twente, Enschede, The Netherlands; and §Physical and Chemical Insights Group, Unilever R&D, Port Sunlight, United Kingdom

ABSTRACT Transmembrane pore formation is central to many biological processes such as ion transport, cell fusion, and viral infection. Furthermore, pore formation in the ceramide bilayers of the stratum corneum may be an important mechanism by which penetration enhancers such as dimethylsulfoxide (DMSO) weaken the barrier function of the skin. We have used the potential of mean constraint force (PMCF) method to calculate the free energy of pore formation in ceramide bilayers in both the innate gel phase and in the DMSO-induced fluidized state. Our simulations show that the fluid phase bilayers form archetypal water-filled hydrophilic pores similar to those observed in phospholipid bilayers. In contrast, the rigid gel-phase bilayers develop hydrophobic pores. At the relatively small pore diameters studied here, the hydrophobic pores are empty rather than filled with bulk water, suggesting that they do not compromise the barrier function of ceramide membranes. A phenomenological analysis suggests that these vapor pores are stable, below a critical radius, because the penalty of creating water-vapor and tail-vapor interfaces is lower than that of directly exposing the strongly hydrophobic tails to water. The PMCF free energy profile of the vapor pore supports this analysis. The simulations indicate that high DMSO concentrations drastically impair the barrier function of the skin by strongly reducing the free energy required for pore opening.

INTRODUCTION

The formation of transient pores in lipid bilayers is central to many biological processes including the transport of molecules and ions across membranes, apoptosis, membrane fusion, and drug and gene delivery (1–4). Recent experiments and computer simulations (5–13) of protein-free bilayers in the fluid phase have provided new insights in the localized density perturbations of membranes and the ensuing formation of transmembrane pores. In this article, we use molecular dynamics (MD) simulations to study pore formation in ceramide bilayers in both the fluid and the gel phase. The membrane in the fluid phase is found to develop hydrophilic pores, i.e., the membrane edge consists of the hydrophilic headgroups of the lipids, which are readily filled with water molecules. On the other hand, the bilayer in the gel phase gives rise to hydrophobic pores, i.e., pores lined by the hydrophobic lipid tails. This highly hydrophobic environment prevents bulk water from entering the pore, at least for pore radii well below the membrane thickness. Observations of a similar nature including evacuation and condensation of water in confined hydrophobic cavities have also been reported in simulations of membrane-spanning conduction channels in biomimetic models of proteins (14–17). The current study on protein-free transmembrane pores builds on these earlier insights.

In this work, we consider bilayers of ceramide 2 lipids, which comprise two long-chain hydrocarbon tails and a small hydrophilic headgroup (see Fig. 1). At the cellular level, ceramides play a key role in signal transduction where they are involved in the regulation of the cell growth cycle (18–20). Ceramides are also a primary constituent of the topmost layer of the skin, the stratum corneum, where they play a pivotal role in the skin's barrier function (21). Ceramide 2 is the most abundant of the ceramides present in the skin. In transdermal delivery, one must overcome this barrier to deliver active molecules into or via the skin. One approach is to use chemical penetration enhancers such as dimethylsulfoxide (DMSO, see Fig. 1), which increase the permeability of the skin (22). In our previous work, we showed that DMSO, in high concentrations, induces a transition in ceramide bilayers from the gel phase to the fluid phase, which can explain the increase in the permeability of these membranes to solutes (23). Another possible mechanism by which DMSO can enhance membrane permeability is transmembrane pore formation, as DMSO is known to induce spontaneous pore formation in phospholipid bilayers (24,25). An understanding of possible mechanisms of pore formation in the skin lipid membranes will be invaluable toward developing controlled transdermal delivery systems. Of a wider interest is the general understanding of pore formation in membranes, as pores play an important role in many biological processes in living cells.

SIMULATION DETAILS

In this study, we use the potential of mean constraint force (PMCF) method (26–28) to calculate the free energy of pore formation in ceramide 2 bilayers in pure water (gel phase) and in 0.6 mol fraction DMSO (fluid phase). The PMCF method enables one to calculate the free energy change of any given process as a function of some reaction coordinate ξ by performing a series of

Submitted May 27, 2008, and accepted for publication August 11, 2008.

Address reprint requests to Wouter K. den Otter, Tel.: 31-53-489-2441; E-mail: w.k.denotter@utwente.nl.

Rebecca Notman's present address is Dept. of Chemistry, University of Warwick, Coventry, UK.

Editor: Peter Tieleman.

0006-3495/08/11/4763/09 $2.00

doi: 10.1529/biophysj.108.138545

FIGURE 1 Molecular structures of ceramide 2 and dimethylsulfoxide (DMSO).

simulations at discrete values of ξ. In this case, we use a coordinate based on the local lipid density in the center of the bilayer to calculate the free energy profile $F_{\mathrm{PMCF}}(\xi)$ of an emerging pore. The reader is referred to the literature (6,7) for a detailed explanation of the method. In our simulations, the value of the reaction coordinate is varied in a number of steps from zero, which corresponds to the equilibrium lipid density in an unconstrained bilayer, to a value close to the maximum of one, where the centers of mass of all the lipids are pushed nearly 1.5 nm from the center of the pore. To convert the resulting free energy profile $F_{\mathrm{PMCF}}(\xi)$ into a function $F(R)$ of the pore radius R, we use a modified particle insertion routine to establish a relation $R(\xi)$ between the pore radius and the central lipid density (6). In particular, for ξ-values approaching zero, where the bilayer no longer contains a true pore, the function $R(\xi)$ makes a smooth transition to a straight line that reaches $R = 0$ at $\xi = 0$. We emphasize that in the MD simulations there are no restrictions on the configurations or orientations of the lipids themselves: all atoms are completely free to move about within the single constraint of a fixed reaction coordinate. The constraint merely determines the size of the pore, but does not affect its shape or hydrophobicity. The ceramides and solvent molecules together determine the preferred pore geometry at any given value of ξ, by minimizing the system's free energy in the presence of an internal constraint.

We performed constrained MD simulations on ceramide bilayers of 512 lipids, in pure water and in an aqueous solution containing 0.6 mol fraction DMSO, both at a temperature of 323 K. The ratio of lipid to solvent (water or DMSO) was 1:40. The united-atom force field for the ceramides was based on the force field of Berger et al. (29), with adjusted partial charges for the headgroup. The united-atom DMSO model was parameterized by Bordat et al. (30), and the water was simulated using the SPC model (31). These force-field and simulation parameters were identical to those used in our previous simulations of ceramide bilayers in water/DMSO mixtures (23), and we refer to that study for further simulation details. The initial configurations of each system were generated by replicating equilibrated bilayers of 128 lipids from a previous set of simulations (23). The area per lipid was kept constant at 0.390 and 0.675 nm^2 for the bilayers with 0 and 0.6 mol fraction DMSO, respectively. These areas are the equilibrium area per lipid obtained from simulations of 128 lipids in the NPT ensemble; a subsequent set of simulations in the NAP_ZT ensemble, exploring a range of areas, has meanwhile improved the equilibrium area of the crystalline state to 0.374 nm^2 (23). All the simulations were performed using a version of GROMACS (32) that had been modified to constrain the reaction coordinate ξ. Applying this constraint in combination with a barostat on the lateral membrane dimension creates several complications, i.e., the constraint force contributes to the lateral pressure and rescaling the lateral box dimension alters the value of the reaction coordinate, which we avoided by performing the simulations at constant area. There are no couplings between the reaction coordinate and the barostat perpendicular to the membrane, as both operate along orthogonal directions, hence the perpendicular pressure was set at 1 bar. By running simulations in the NAP_ZT ensemble, the solvent at some distance from the membrane acquired a hydrostatic pressure of 1 bar, while the membrane was exposed to distinct lateral and perpendicular pressures and therefore experienced a surface tension.

THEORY

Theoretical ideas of pore formation in membranes are dominated by classical nucleation theory. In the phenomenological model of Litster (33), the membrane is assumed to be a two-dimensional elastic medium with a circular hole. The membrane is characterized by a free energy per unit area γ_S more commonly known as the surface tension, while the membrane edge forming the circumference of the pore is characterized by a free energy per unit length of the bilayer edge or line tension λ. In this mesoscopic model, the free energy difference between an intact membrane and one containing a pore of radius R is given by

$$\Delta F = 2\pi R\lambda - \pi R^2\gamma_S. \tag{1}$$

The model yields an activation barrier of $\Delta F(R^*) = \pi\lambda^2/\gamma_S$ and predicts that pores with a radius of less than a critical value of $R^* = \lambda/\gamma_S$ will reseal. Larger pores will grow indefinitely, because the surface tension is assumed to remain constant while the pore grows. A mesoscopic free energy expression of the bilayer, which includes the effects of variations in the tension, and thus permits stable pores, is given by Tolpekina et al. (5):

$$F_{\mathrm{philic}}(R) = \frac{K_A}{2A_0}(A - A_0)^2 + 2\pi R\lambda. \tag{2}$$

Here, the first term on the right-hand side takes into account the free energy cost associated with the reduction of the area per lipid when a pore is created at constant ground plane area $A_\parallel$ of the simulation box. K_A is the elastic modulus, A_0 is the equilibrium bilayer area in the tensionless state, and $A = A_\parallel - \pi R^2$ is the actual area of the bilayer calculated by subtracting the area of the pore from the ground plane area of the box. This model predicts that pores are unstable and reseal below a critical elongation. Above this elongation, a pore still has to surmount an activation barrier before free energy minimalization starts to drive the growth of the pore. Due to the fixed ground plane area, the growing pore reduces the surface tension, $\gamma_S = \partial F_{\mathrm{philic}}/\partial A_\parallel$, and the pore expansion will stop when a further decrease in elastic energy is balanced by an increase of edge energy. This minimum in the free energy evidently occurs at a pore area smaller than the excess area, $\pi R_{\mathrm{eq}}^2 < A_\parallel - A_0$ with a residual tension of $\gamma_S = \lambda/R_{\mathrm{eq}}$. The free energy rises indefinitely for larger pore radii. We refer to Tolpekina et al. (5) for a detailed discussion of the model's properties.

In both free energy models, the pore radius at the activation barrier is related to the prevalent surface tension by λ/γ_S. Both free energy models yield nearly identical activation barriers for the giant unilamellar vesicles at several percent elongation typically used in rupture experiments (9). Beyond this barrier, a pore grows large by thermodynamical driving forces. In the model by Tolpekina et al., this growth eventually stops, but the resulting pore in the vesicle will be huge. If an externally applied force maintains a constant surface tension, as in the Litster model, then the pore area and the ground plane area will obviously grow indefinitely. Litster's model emerges from Eq. 2 for stretched membranes, $A_\parallel > A_0$,

as the Taylor expansion of $\Delta F = F_{\text{philic}}(R) - F_{\text{i}}$ to second-order in R as long as the pore is sufficiently small relative to the excess area, $\pi R^2 \ll A_{\|} - A_0$, for the surface tension to be effectively constant at $\gamma_{\text{S}} = K_{\text{A}}(A_{\|} - A_0)/A_0$, and $F_{\text{i}} = K_{\text{A}}(A_{\|} - A_0)^2/(2A_0)$ denotes the free energy of the intact membrane. A more detailed discussion of the relation between these two phenomenological models is presented elsewhere (W. K. den Otter, in preparation).

As mentioned in the previous section, we have chosen to perform the simulations at constant lateral area for computational reasons. The simulation results are therefore interpreted using the free energy of Eq. 2 to determine the properties of the porated membrane. Since previous simulations indicate that the line tension is essentially independent of the surface tension (5), the two phenomenological expressions may then be used to translate the results to different conditions, like another ground plane area or an ensemble of constant tension. Being of mesoscopic origin, both expressions for the free energy may fail when microscopic details become relevant, i.e., for pore radii comparable to the membrane thickness. In this region, there is no established theory available with which to compare our PMCF calculations.

RESULTS

Hydrophilic pore

The constraint on the local lipid density of the ceramide bilayer in the DMSO-induced fluidized phase results in the formation of an archetypal hydrophilic pore, as shown in Fig. 2. At small values of ξ or low radii ($\xi < 0.38$, equivalent to $R < 0.05$ nm), the lipid density decreases with increasing ξ, while the surfaces of the bilayer begin to move inwards and some headgroups and DMSO molecules move into the center of the low-density region. At $\xi = 0.63$, equivalent to $R = 0.07$ nm, the headgroups of opposing monolayers make contact and a hydrophilic pore, which is concomitantly filled with DMSO and water, opens up in the bilayer. The radius of the transmembrane pore then increases further with increasing ξ. This mechanism is consistent with that observed for coarse-grained lipids (6) and phospholipids (7), where a hydrophilic pore was formed in a bilayer using the same method.

The free energy as a function of pore radius was determined as described previously (6,7) and is plotted in Fig. 3. The free energy is quadratic in the radius below $R = 0.06$ nm, the region which corresponds to the gradual reduction of the density in the center of the still intact membrane. Beyond $R = 0.06$ nm, for membranes exhibiting a real pore, the free energy increases slower with increasing pore radius. A fit of Eq. 2 to the results for the ceramide bilayer with 0.6 mol fraction DMSO yields a line tension coefficient λ of 6 pJ/m, an elastic modulus K_{A} of 260 mJ/m^2, and an equilibrium area per lipid a_0 of 0.65 nm^2. The latter two results are in good agreement with the mechanical properties in our previous *NPT* simulations of the same system (23) (see Table 1). A low free energy barrier to pore formation of only a few $k_{\text{B}}T$ indicates that DMSO can promote spontaneous pore formation, in agreement with previous simulations on other lipid bilayers (24,25,34).

To validate the line tension obtained from the constrained simulations, we performed separate simulations of a strip of 512 lipids in a bilayer, surrounded by solvent molecules in the normal direction and one of the lateral directions, as detailed in Tolpekina et al. (5). The ground-plane dimensions L_{x} and L_{y} of the simulation box were fixed, while the box length L_{z} in the normal (z) direction was allowed to adjust to

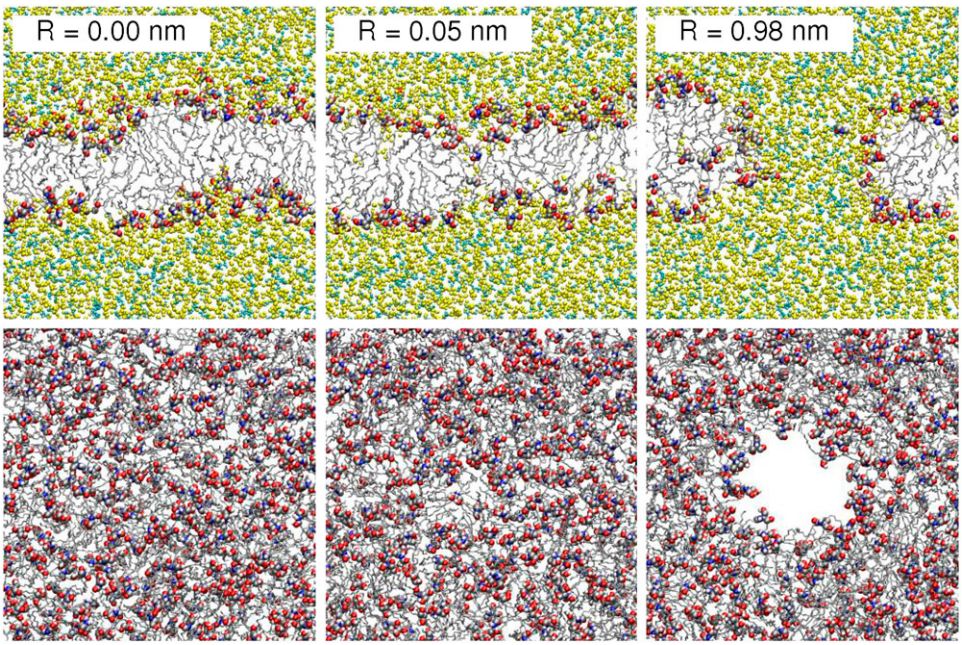

FIGURE 2 By mechanically constraining the lipid density in the center of a fluidized ceramide 2 bilayer in a 0.6 mol fraction DMSO solvent, a hydrophilic transmembrane pore of radius R is created. Snapshots are shown of a slice of the bilayer through the center of the pore (center of box) and of a top-down view of the bilayer (shown without water). Water is colored cyan, DMSO yellow, and ceramide carbon atoms are colored gray, nitrogen atoms blue, oxygen atoms red, and hydrogen atoms white.

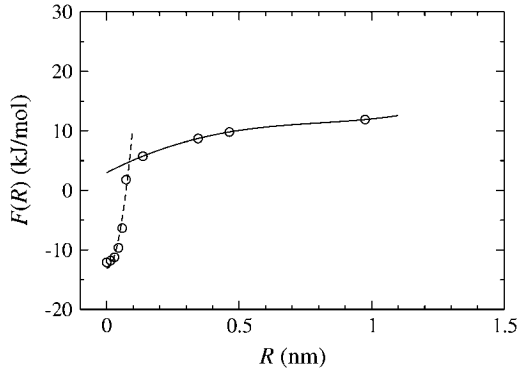

FIGURE 3 Free energy $F(R)$ as a function of pore radius R for the ceramide bilayer with 0.6 mol fraction DMSO. The solid line shows the fit of the data to Eq. 2 for bilayers with a transmembrane pore; the dashed line is a quadratic fit for the intact membranes with a strong local lipid-density reduction.

maintain a pressure of 1 bar. The system was equilibrated for 5 ns and this was followed by a 5-ns production run. The line tension λ was calculated from the pressure difference as $\lambda = 1/2\, L_z\, L_y\, (P_{xx} + P_{yy} - 2P_{zz})$, where P_{xx}, P_{yy}, and P_{zz} are the diagonal elements of the pressure tensor and the factor 1/2 accounts for the two edges of the strip. For the ceramide bilayer in the fluid phase, i.e., at 0.6 mol fraction DMSO, we obtained a value for the line tension of 7 pJ/m (see Table 1), which is in good agreement with the value of 6 pJ/m obtained from the constrained simulations as described above.

The good fit of the simulation data in Fig. 3, in combination with the good agreement between the fit parameters and their independently established values, indicates that the free energy of pore formation at constant area $A_\parallel$ is well described by Eq. 2. As in previous studies (6,7), the theory holds true down to remarkably low pore radii of ~0.1 nm. The thermodynamic description of perforated membranes beyond this radius is therefore readily converted to an ensemble with an alternative area or with a constant tension, using Eq. 2 and 1, respectively, to arrive at the appropriate free energy curve in the second ensemble. Below this radius, in the absence of a clearcut pore and without the advantage of established free energy expressions, one has to rerun the simulations under the conditions of the new ensemble. Since the nascent pore is very small relative to the simulated membrane patch, it appears to be justifiable at these diminutive radii to equate a constant tension ensemble to a constant area ensemble with $A_\parallel = A_0 + \gamma_S\, A_0/K_A$ for computational convenience.

TABLE 1 Impact of DMSO concentration on the mechanical properties of a ceramide 2 membrane

Mol fraction of DMSO	a_0 (nm^2)	K_A (mJ/m^2)	λ (pJ/m)
0.0	0.374 ± 0.001	7900 ± 700	440 ± 8
0.1	0.385 ± 0.001	3700 ± 300	250 ± 20
0.6	0.68 ± 0.02	190 ± 20	7 ± 20

The equilibrium area per lipid $a_0 = 2A_0/N$ and the elastic modulus K_A are obtained from *NPT* simulations.(23) The line tension λ is calculated from simulations of a bilayer strip, as described in the text.

Hydrophobic pore

We next consider the ceramide bilayer in pure water, where a strong interlipid network with three hydrogen bonds per headgroup gives rise to a gel phase of hexagonally ordered ceramides (23). The rigidity of this phase strongly affects the pore opening process, as can be seen in Fig. 4. At small values of ξ ($\xi < 0.31$, equivalent to $R < 0.02$ nm), the lipid density in the center of the bilayer steadily decreases with increasing ξ. This is also evident as an increase in the disorder of the ceramide tails in the center of the pore. As ξ increases to 0.46 ($R = 0.03$ nm), the interactions between ceramide headgroups surrounding the nascent pore are broken gradually, and a cavity, partially filled with lipid tail groups, forms in the bilayer. At $\xi = 0.46$, a full transmembrane pore opens up in the bilayer, after which the radius of the pore increases with increasing ξ. The strong bindings between the ceramides in the gel phase prevent the lipids surrounding the pore from rearranging into a smoothly rounded membrane edge. In the resulting hydrophobic pore, the hydrophobic tails at the edge of the membrane are exposed to the solvent, whereas, in the hydrophilic pore at 0.6 mol fraction DMSO, the hydrophilic heads are lining the interior of the pore to shield the tails from the solvent. Textbook cartoons of the two distinct pore structures are shown in Fig. 5 to illustrate the difference in the membrane-solvent interfaces encompassing the pore. In contrast to this common conception of the interior makeup of a hydrophobic pore, the simulations show that the water molecules do not spontaneously enter the interior of the pore, even when the pore is large enough to accommodate many water molecules (see Fig. 4). This situation persists until the termination of the simulation after 5 ns, suggesting that a water vapor region inside the pore is able to coexist in equilibrium with the bulk water that surrounds the bilayer. These observations are reminiscent of the situation in hydrophobic protein channels, which are also void at low channel radii (14–17,35,36), and the findings by Tepper and Voth (37) that water molecules do not enter an artificially created transmembrane pore. These pores are hereafter referred to as vapor pores (see Fig. 5), and are discussed in detail below. Note that due to the small volume of the pore, at the set (ambient) pressure the vapor pores are actually devoid of water molecules for most of the time and therefore appear empty in the snapshots.

The free energy of pore formation in the gel-phase bilayer as a function of the radius of the pore is presented in Fig. 6. As with the fluidized bilayer at 0.6 mol fraction DMSO, there are two clearly distinguishable regions. Below $R = 0.03$ nm, the free energy associated with reducing the density in the center of the bilayer is again nearly quadratic in the radius. At $\xi = 0.46$, $R = 0.03$ nm, a transmembrane pore opens up,

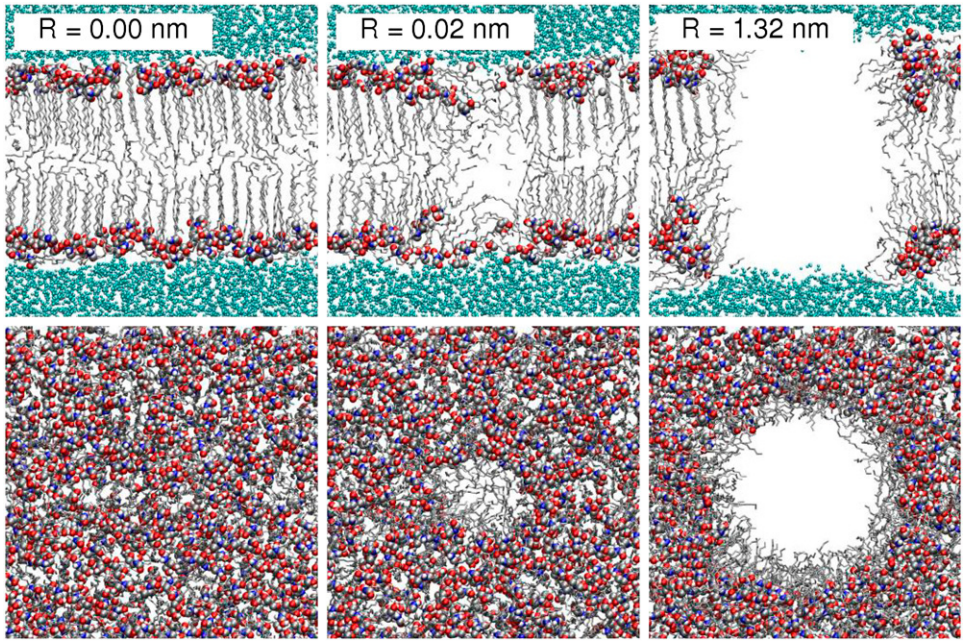

FIGURE 4 Effect of the constraint on the ceramide bilayer without DMSO, where R is the radius of the pore. Snapshots are shown of a slice of the bilayer through the center of the pore (center of box) and of a top-down view of the bilayer (shown without water). Water is colored cyan and ceramide carbon atoms are colored gray, nitrogen atoms blue, oxygen atoms red, and hydrogen atoms white.

concomitant with the transition to a much slower free energy increase with increasing pore radius. Note that the free energy change required until pore opening is one order higher in the gel phase than in the fluidized phase, mainly because the bonds between the ceramides are considerably stronger than in the fluidized phase (23) (which is also reflected by the higher elastic modulus, see Table 1). Stimulated by several successful descriptions of molecular-size hydrophilic pores by the mesoscopic theory of Eq. 2 and mesoscopic models of hydrophobic pores in protein channels by Beckstein and coworkers (14–17), and Allen et al. (35,36), we expect that mesoscopic theories can also be used to describe the free energies of hydrophobic and vapor pores. For a rigid bilayer, where the energetic cost of rearranging the lipids is high, the formation of a hydrophobic pore may be preferable over a hydrophilic pore. As illustrated in Fig. 5, the hydrophobic pore has an approximately cylindrical interface between the hydrocarbon tails and the water in the pore. Thus, we replace the line tension term in Eq. 2 with the free energy cost of the tail-water interface, to yield an expression for the free energy of a hydrophobic pore:

$$F_{\text{phobic}}(R) = \frac{K_A}{2A_0}(A - A_0)^2 + 2\pi R h \gamma_{tw}. \qquad (3)$$

Here, h is the height of the membrane and γ_{tw} is the free energy cost per unit area or surface tension of the tail-water interface. A similar derivation applied to the vapor pore, which has a cylindrical tail-vapor interface and two circular water-vapor interfaces, gives

$$F_{\text{vapor}}(R) = \frac{K_A}{2A_0}(A - A_0)^2 + 2\pi R h \gamma_{tv} + 2\pi R^2 \gamma_{wv}, \qquad (4)$$

where γ_{tv} and γ_{wv} are the free energies per unit area of the tail-vapor interface and the water-vapor interface, respectively. The work associated with pore formation, $PV \approx P_z \pi R^2 h$, has been ignored here, as it is several orders smaller than the included terms. The free energies of the hydrophobic pore and vapor pore are identical for a critical radius $R_c = h(\gamma_{tw} - \gamma_{tv})/\gamma_{wv}$. By inserting the experimental values (38) of the water-vapor surface tension, $\gamma_{wv} = 72.8$ mJ/m^2, the n-octane-vapor surface tension $\gamma_{tv} = 21.8$ mJ/m^2, and the n-octane-water surface tension $\gamma_{tw} = 50.8$ mJ/m^2, one arrives at $R_c \approx 0.4\,h$. Since γ_{tw} is larger that γ_{tv}, it follows that small hydrophobic pores, $R < R_c$, contain only water vapor. Our simulations, with pore radii up to 1.3 nm in a rigid membrane of ~5 nm thickness, are within this regime. Only large hydrophobic pores, $R > R_c$, are expected to hold fluid water.

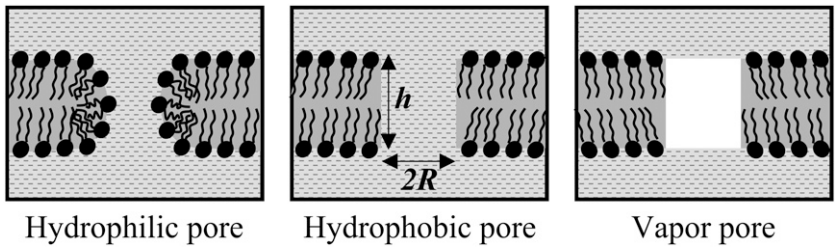

FIGURE 5 Cartoons of pore structures. A hydrophilic pore is formed when the hydrophilic headgroups rearrange to shield the hydrocarbon tails from the water. In a hydrophobic pore, the headgroups do not rearrange and the tails are exposed to the water. In a vapor pore, water does not enter the interior of the pore.

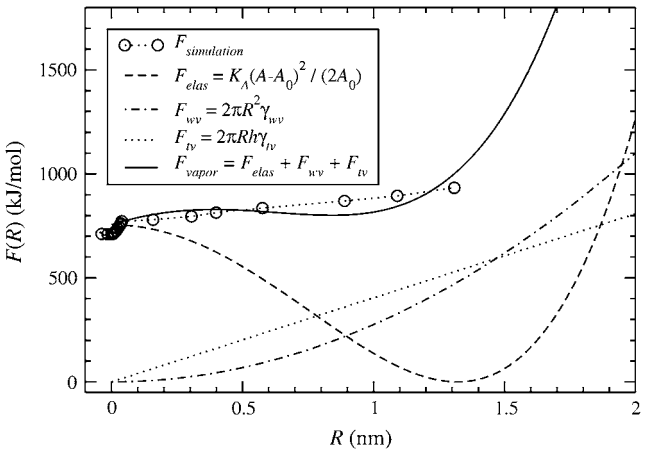

FIGURE 6 Free energy $F(R)$ as a function of pore radius R for the ceramide bilayer in the gel phase. Also shown are the elastic F_{elas}, water-vapor F_{wv}, and tail-vapor F_{tv} contributions to the total free energy F_{vapor}.

The elastic, water-vapor, and tail-vapor contributions to the free energy $F_{vapor}(R)$ of a vapor pore are presented as three separate curves in Fig. 6. To generate these plots we used our previously established values of K_A and A_0 (see Table 1), and the aforementioned experimental values (38) of the water-vapor and *n*-octane-vapor surface tensions. Each component of the free energy shows a strong variation with R, yet the summed result $F_{vapor}(R)$ is in reasonable agreement with the simulation results (see Fig. 6). In plotting the latter curve, the free energy $F_i(A_{||})$ of the intact membrane has been used as the reference point for the PMCF free energy difference calculations (26–28) in the thermodynamically consistent way outlined in Tolpekina et al. (6). It appears, therefore, that the mesoscopic model holds down to very small pore radii, where molecular effects become relevant. Compared to the theoretical curve, the simulation data show only small deviations from linearity, which prohibits a reliable fit with the fourth-order polynomial $F_{vapor}(R)$. We further note that as the ceramides are packed in the ordered gel phase, there are likely to be internal free energies associated with lattice faults and deformation stresses introduced by the pore. Such free energy costs are not accounted for in the simple expression $F_{vapor}(R)$ for the vapor pore.

At this point, it is worth iterating that the observed vapor pore is not related to the applied constraint, nor to the employed thermodynamic ensemble. The solvent does not partake in the constraint, and the lipids are free to adopt their preferred orientations under the lateral forces exerted by the constraint. A barostat on the perpendicular direction ensures a hydrostatic pressure of 1 bar in the solvent, which apparently does not suffice to push the water molecules into the hydrophobic cavity. Laplace's law yields a radius of curvature for the water-vapor interface of $\sim 3.6 \times 10^{-7}$ m, which confirms the flatness of these interfaces in the snapshot of Fig. 4. With increasing pore radius, the tension on the membrane samples a range of values down to approximately zero at $R = 1.35$ nm, but this does not alter the shape of the membrane edge. On the collective basis of the preceding arguments, we believe that vapor pores are an inherent feature of ceramide bilayers and are probably a generic property of membranes in the gel phase.

To further verify our results, we performed two additional 5-ns simulations of perforated bilayers with pore radii of $R =$ 0.6 and 1.3 nm, where the starting configurations were generated by redistributing the water molecules over the available volume, including the interior of the pore. In the simulation of the smaller pore, the water molecules diffused out of the pore within 0.2 ns and the pore remained empty for the remainder of the simulation. In contrast, the larger pore remained filled with water for the duration of the simulation, with water molecules in continuous exchange between the bulk and the interior of the pore. Firstly, these simulations confirm that the dynamics of the water molecules is fast enough for them to diffuse into or out of the pore over the timescale of the current simulations, and support the idea that a vapor pore rather than a hydrophobic pore is the most stable arrangement of the system for pores with a radius well below a critical radius R_c. Secondly, the simulations suggest that there is an activation barrier associated with the transitions between a hydrophobic pore and a vapor pore for a radius close to R_c; the large $R = 1.3$ nm pore does not spontaneously fill with water and neither do artificially inserted water molecules evacuate the pore immediately. These considerations also suggest some hysteresis, at least on the timescales accessible in MD simulations, in the filling and evacuation of small pores with unshielded tails. Similar observations were made in the filling and evacuation of hydrophobic protein channels (14,35).

The line tensions of the ceramide bilayers calculated from simulations of a bilayer strip (5,39) are given in Table 1. As expected, the lipids in the ceramide bilayer with 0.6 mol fraction DMSO rearrange so that their headgroups shield the tails from the water (Fig. 7 *c*). The line tension of 7 pJ/m is comparable to typical experimental values of the line tension of bilayers in the fluid phase (40–44). The bilayer strip of ceramides in pure water favors a hydrophobic arrangement of the two membrane edges flanking a gel phase core (see Fig. 7 *a*). Due to the exposure of the hydrophobic tails to the water, Fig. 7, the line tension of the gel-phase bilayer is 440 ± 8 pJ/m, which is significantly higher than that of the fluid phase. It appears that the high line tension is a result of the conflict between the cost of forming unfavorable hydrocarbon-water contacts and the rigidity of the bilayer, i.e., the conflict that also prevents the gel phase from forming a hydrophilic pore. However, in contrast to the tail-lined pores, in the current geometry the exposed tails will not be cushioned from the water by a layer of vapor because the resulting free energy per unit edge area, which would amount to $\sim(\gamma_{tv} + \gamma_{vw})$, exceeds the γ_{tw} of exposing tails directly to the water. As an aside, we also calculated the line tension of a strip of ceramide bilayer in

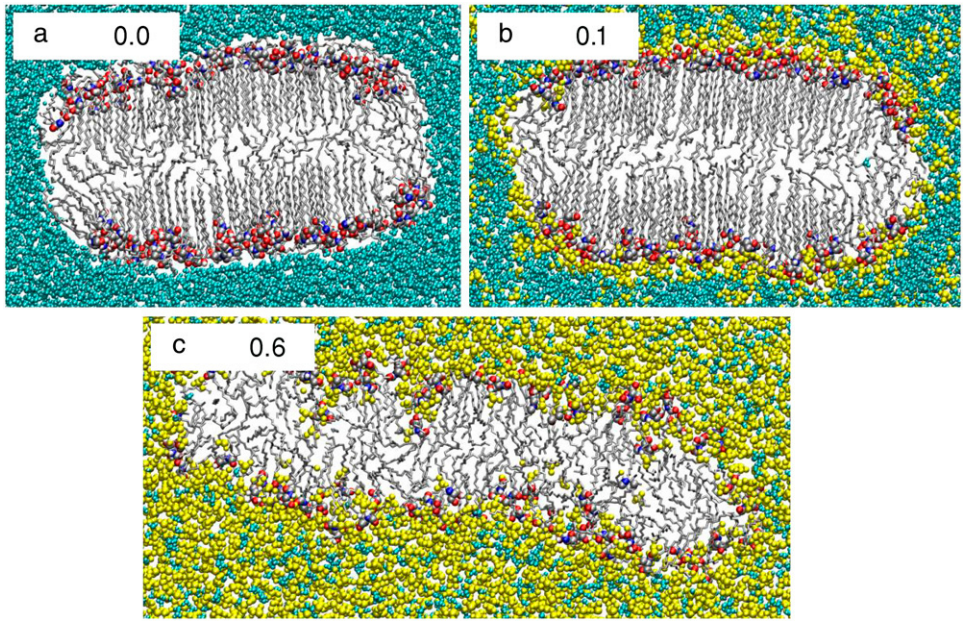

FIGURE 7 Snapshots of a slice through the strips of bilayer in (*a*) pure water, (*b*) 0.1 mol fraction DMSO, and (*c*) 0.6 mol fraction DMSO, showing the bilayer edge.

0.1 mol fraction DMSO where the bilayer is also in the rigid gel phase. In this case, the headgroups do not rearrange and the edge is still hydrophobic; however, the line tension drops to 250 ± 20 pJ/m due to the accumulation of DMSO molecules at the tail-water interface, where they shield the tails from the water (see Fig. 7 *b*).

DISCUSSION AND CONCLUSIONS

We have used molecular dynamics simulations to study pore formation in a ceramide 2 bilayer in water, which serves as a model of the nearly impermeable upper layer of the skin. In their natural state, the ceramides are densely packed in a highly rigid gel phase, stabilized by a strong network of hydrogen bonds connecting the headgroups. The resulting immobilization of the ceramides prevents the rearrangement of the lipids near a membrane edge, which consequently leaves the hydrophobic tails exposed to the solvent. Simulations of this unfavorable membrane rim, using a bilayer strip with two straight edges, yield a line tension approximately two orders higher than the typical values reported for fluid membranes. A transmembrane pore with a nanometer radius thus constitutes a narrow highly hydrophobic cavity, making it unattractive for water molecules to enter the pore. The simulations show that these small pores are only filled with water vapor, and hence are effectively empty, as are tight protein channels with an equally hydrophobic lining (14–17). We expect that vapor pores may also exist in other rigid gel-phase bilayers. A phenomenological model, balancing the energies of tail-vapor and water-vapor interfaces against that of a tail-water interface, suggests that hydrophobic pores in a membrane of thickness h are void below a critical radius $R_c \approx 0.4h$ and water-filled above this radius.

The creation of the smallest veritable transmembrane pore ($R \approx 1$ Å) in the gel phase bilayer requires a free energy of $\sim$60 kJ/mol, or slightly $>20\ k_BT$, which is comparable to the value found for DPPC in the fluid phase (7). While in principle this pore can conduct small molecules, in practice the transport of water and water-soluble molecules is effectively blocked by the hydrophobicity of the pore. Enlarging the pore to the aforementioned critical radius, where one expects the pore to become conductive at last, necessitates an extra 1.9 MJ/mol or $>700\ k_BT$ (excluding the elastic energy of the membrane). This high activation energy indicates that transmembrane transport by pores is highly unlikely under the standard condition of near-vanishing lateral tension. The hydrophobicity of the membrane edge, and the resulting formation of vapor pores, appear to play a crucial role in this process by increasing the activation energy by more than an order of magnitude. The gel phase itself is highly impermeable and it appears from the simulations that small defects are unlikely to compromise its barrier function to water, ions, and other polar molecules. We speculate that these insights explain the apparent paradox that the human body should have evolved to employ layers of ceramide-rich membranes as the main barrier between our bodies and the outside world, when such a rigid lipid phase is expected to be highly prone to defects whenever the skin undergoes flexing.

At a high concentration of the potent skin permeability enhancer DMSO, the hydrogen-bonding network between the ceramides is sufficiently weakened to induce a transition in the bilayer from the innate gel phase to a fluid phase. The activation energy for pore formation is drastically reduced: a mere 20 kJ/mol or $7\ k_BT$ suffices to open a 1 Å pore. The mobility of the lipids permits the formation of a smooth and continuous layer of headgroups, which shields the tails from

the water at the bilayer edge, to yield a hydrophilic pore. Water molecules readily enter such a pore, making it conductive even at a low radius. Due to the reduced line tension, it takes relatively little energy to enlarge the pore to accommodate a higher flux. Molecular diffusion across the bilayer is also easier in the thinner and less dense fluidized state than in the gel phase. Future challenges include studies to understand the mechanisms of action of other permeability enhancers in the search for safe and widely applicable transdermal delivery systems.

This work was funded by the Engineering and Physical Sciences Research Council and Unilever Research. The authors acknowledge SoftComp European Union Network of Excellence for providing support to one of us (R.N.) to perform part of this work at the University of Twente (Eurothesis Program).

REFERENCES

1. Cohen, F. S., and G. B. Melikyan. 2004. The energetics of membrane fusion from binding, through hemifusion, pore formation, and pore enlargement. *J. Membr. Biol.* 199:1–14.
2. Cevc, G. 2004. Lipid vesicles and other colloids as drug carriers on the skin. *Adv. Drug Deliv. Rev.* 56:675–711.
3. Tieleman, D. P. 2006. Computer simulations of transport through membranes: passive diffusion, pores, channels and transporters. *Clin. Exp. Pharmacol. Physiol.* 33:893–903.
4. Javadov, S., and M. Karmazyn. 2007. Mitochondrial permeability transition pore opening as an endpoint to initiate cell death and as a putative target for cardioprotection. *Cell. Physiol. Biochem.* 20:1–22.
5. Tolpekina, T. V., W. K. den Otter, and W. J. Briels. 2004. Simulations of stable pores in membranes: system size dependence and line tension. *J. Chem. Phys.* 121:8014–8020.
6. Tolpekina, T. V., W. K. den Otter, and W. J. Briels. 2004. Nucleation free energy of pore formation in an amphiphilic bilayer studied by molecular dynamics simulations. *J. Chem. Phys.* 121:12060–12066.
7. Wohlert, J., W. K. den Otter, O. Edholm, and W. J. Briels. 2006. Free energy of a trans-membrane pore calculated from atomistic molecular dynamics simulation. *J. Chem. Phys.* 124:154905.
8. Farago, O., and C. D. Santangelo. 2005. Pore formation in fluctuating membranes. *J. Chem. Phys.* 122:044901.
9. Evans, E., V. Heinrich, F. Ludwig, and W. Rawicz. 2003. Dynamic tension spectroscopy and strength of biomembranes. *Biophys. J.* 85:2342–2350.
10. Melikov, K. C., V. A. Frolov, A. Shcherbakov, A. V. Samsonov, and Y. A. Chizmadzhev. 2001. Voltage-induced nonconductive pre-pores and metastable single pores in unmodified planar lipid bilayer. *Biophys. J.* 80:1829–1836.
11. Loison, C., M. Mareschal, and F. Schmid. 2004. Pores in bilayer membranes of amphiphilic molecules: coarse-grained molecular dynamics simulations compared with simple mesoscopic models. *J. Chem. Phys.* 121:1890–1900.
12. Tieleman, D. P., H. Leontiadou, A. E. Mark, and S. J. Marrink. 2003. Simulation of pore formation in lipid bilayers by mechanical stress and electric fields. *J. Am. Chem. Soc.* 125:6382–6383.
13. Wang, Z. J., and D. Frenkel. 2005. Pore nucleation in mechanically stretched bilayer membranes. *J. Chem. Phys.* 123:154701.
14. Beckstein, O., P. C. Biggin, and M. S. P. Sansom. 2001. A hydrophobic gating mechanism for nanopores. *J. Phys. Chem. B.* 105: 12902–12905.
15. Beckstein, O., and M. S. P. Sansom. 2006. A hydrophobic gate in an ion channel: the closed state of the nicotinic acetylcholine receptor. *Phys. Biol.* 3:147–159.
16. Beckstein, O., and M. S. P. Sansom. 2004. The influence of geometry, surface character, and flexibility on the permeation of ions and water through biological pores. *Phys. Biol.* 1:42–52.
17. Beckstein, O., and M. S. P. Sansom. 2003. Liquid-vapor oscillations of water in hydrophobic nanopores. *Proc. Natl. Acad. Sci. USA.* 100: 7063–7068.
18. Hauser, J. M. L., B. M. Buehrer, and R. M. Bell. 1994. Role of ceramide in mitogenesis induced by exogenous sphingoid bases. *J. Biol. Chem.* 269:6803–6809.
19. Perry, D. K., and Y. A. Hannun. 1998. The role of ceramide in cell signaling. *Biochim. Biophys. Acta.* 1436:233–243.
20. Kronke, M. 1999. Biophysics of ceramide signaling: interaction with proteins and phase transition of membranes. *Chem. Phys. Lipids.* 101:109–121.
21. Bouwstra, J. A., F. E. R. Dubbelaar, G. S. Gooris, and M. Ponec. 2000. The lipid organization in the skin barrier. *Acta Derm. Venereol.* 80:23–30.
22. Williams, A. C., and B. W. Barry. 2004. Penetration enhancers. *Adv. Drug Deliv. Rev.* 56:603–618.
23. Notman, R., W. K. den Otter, M. G. Noro, W. J. Briels, and J. Anwar. 2007. The permeability enhancing mechanism of DMSO in ceramide bilayers simulated by molecular dynamics. *Biophys. J.* 93: 2056–2068.
24. Notman, R., M. Noro, B. O'Malley, and J. Anwar. 2006. Molecular basis for dimethylsulfoxide (DMSO) action on lipid membranes. *J. Am. Chem. Soc.* 128:13982–13983.
25. Gurtovenko, A. A., and J. Anwar. 2007. Modulating the structure and properties of cell membranes: the molecular mechanism of action of dimethyl sulfoxide. *J. Phys. Chem. B.* 111:10453–10460.
26. den Otter, W. K., and W. J. Briels. 1998. The calculation of free-energy differences by constrained molecular-dynamics simulations. *J. Chem. Phys.* 109:4139–4146.
27. den Otter, W. K. 2000. Thermodynamic integration of the free energy along a reaction coordinate in Cartesian coordinates. *J. Chem. Phys.* 112:7283–7292.
28. Schlitter, J., and M. Klähn. 2003. A new concise expression for the free energy of a reaction coordinate. *J. Chem. Phys.* 118:2057–2060.
29. Berger, O., O. Edholm, and F. Jahnig. 1997. Molecular dynamics simulations of a fluid bilayer of dipalmitoylphosphatidylcholine at full hydration, constant pressure, and constant temperature. *Biophys. J.* 72:2002–2013.
30. Bordat, P., J. Sacristan, D. Reith, S. Girard, A. Glattli, and F. Muller-Plathe. 2003. An improved dimethyl sulfoxide force field for molecular dynamics simulations. *Chem. Phys. Lett.* 374:201–205.
31. Berendsen, H. J. C., J. P. M. Postma, W. F. van Gunsteren, and W. F. Hermans. 1981. Interaction models for water in relation to protein hydration. *In* Intermolecular Forces. B. Pullman, editor. D. Reidel, Dordrecht, The Netherlands.
32. Lindahl, E., B. Hess, and D. van der Spoel. 2001. GROMACS 3.0: a package for molecular simulation and trajectory analysis. *J. Mol. Model.* 7:306–317.
33. Litster, J. D. 1975. Stability of lipid bilayers and red blood cell membranes. *Phys. Lett. A.* 53:193–194.
34. Moldovan, D., D. Pinisetty, and R. V. Devireddy. 2007. Molecular dynamics simulations of pore growth in lipid bilayer membranes in the presence of edge-active agents. *Appl. Phys. Lett.* 91:204104.
35. Allen, R., J.-P. Hansen, and S. Melchionna. 2003. Molecular dynamics investigation of water permeation through nanopores. *J. Chem. Phys.* 119:3905–3913.
36. Allen, R., S. Melchionna, and J.-P. Hansen. 2002. Intermittent permeation of cylindrical nanopores by water. *Phys. Rev. Lett.* 89:175502.
37. Tepper, H. L., and G. A. Voth. 2005. Protons may leak through pure lipid bilayers via a concerted mechanism. *Biophys. J.* 88:3095–3108.
38. Weast, R. C. (Editor.) 1970. CRC Handbook of Chemistry and Physics. 50 Ed. CRC Press, Cleveland, OH.

39. Jiang, F. Y., Y. Bouret, and J. T. Kindt. 2004. Molecular dynamics simulations of the lipid bilayer edge. *Biophys. J.* 87:182–192.

40. Evans, E., and F. Ludwig. 2000. Dynamic strengths of molecular anchoring and material cohesion in fluid biomembranes. *J. Phys. Condens. Mat.* 12:A315–A320.

41. Loi, S., G. Sun, V. Franz, and H.-J. Butt. 2002. Rupture of molecular thin films observed in atomic force microscopy. II. Experiment. *Phys. Rev. E.* 66:031602.

42. Zhelev, D. V., and D. Needham. 1993. Tension-stabilized pores in giant vesicles: determination of pore size and pore line tension. *Biochim. Biophys. Acta.* 89:1147–1157.

43. Brochard-Wyart, F., P. G. de Gennes, and O. Sandre. 2000. Transient pores in stretched vesicles: role of leak-out. *Physica A.* 278: 32–51.

44. Moroz, J. D., and P. Nelson. 1997. Dynamically stabilized pores in bilayer membranes. *Biophys. J.* 72:2211–2216.